Limit Cycle Oscillations of a Nonlinear Rotorcraft Model

Benson H. Tongue
Georgia Institute of Technology, Atlanta, Georgia

Previous studies of helicopter stability have focused on a linear formulation of the system. This paper addresses the stability question from a nonlinear standpoint. The limit cycle behavior of a rotorcraft having a nonlinear damping characteristic is examined. The effect of parameter variations on the system's response is discussed and differences between a linear and nonlinear model are presented. It is shown that, for the model examined, the nonlinear analysis yields interesting and qualitatively different results from the linear case. A describing function approach is taken to handle the system's nonlinearities. The validity of the approximation is verified by a comparison with numerical simulations of the fully nonlinear equations of motion.

Nomenclature

a = frequency of system's oscillations
$\tilde{a}$ = nondimensional frequency of system's oscillations, $=a/p_0$
C_b = blade damping coefficient
C_0 = fuselage damping coefficient
I = moment of inertia of blade relative to vertical hinge
K_b = rotating blade spring coefficient
K_0 = fuselage spring constant
ℓ_{vh} = vertical hinge offset from rotor axis of rotation
m_0 = mass of fuselage
m_b = mass of blade
M = total mass of craft, $=nm_b+m_0$
n = number of blades
n_b = blade damping coefficient, $=C_b/I$
$\tilde{n}_b$ = nondimensional blade damping coefficient, $=n_b/p_0$
n_0 = fuselage damping coefficient, $=C_0/M$
$\tilde{n}_0$ = nondimensional fuselage damping coefficient, $=n_0/p_0$
p_0 = natural frequency of fuselage on its spring support, $p_0^2=K_0/M$
p_{b_0} = natural frequency of nonrotating blade relative to vertical hinge, $p_{b_0}^2=K_b/I$
S = static imbalance relative to vertical hinge
t = time
x = fuselage motion coordinate
$\tilde{x}$ = nondimensional fuselage motion coordinate, $=x\gamma$
X_0 = amplitude of fuselage coordinate
$\tilde{X}$ = amplitude of nondimensional fuselage coordinate
α_k = angular spacing between arms of rotor
β_k = kth rigid blade
γ = nonlinear fuselage damping coefficient
ϵ = hinged mass ratio, $=(n/2)(S^2/MI)$
η = nonphysical blade coordinate
$\tilde{\eta}$ = nondimensional nonphysical blade coordinate
H_0 = amplitude of nonphysical blade coordinate, $=\eta\gamma(S/M)$
ν_0 = nondimensional blade parameter, $\nu_0^2=\ell_{vh}S/I$
ξ_k = individual blade angular displacement
ρ = mass per unit length of blade
τ = nondimensional time, $=p_0t$
ϕ = nonphysical blade coordinate
$\tilde{\phi}$ = nondimensional nonphysical blade coordinate, $=\phi\gamma(S/M)$
Φ_0 = amplitude of nonphysical blade coordinate
ψ_k = individual blade angular orientation referenced to fuselage, $=\omega t+\alpha_k$
ω = rotor speed
$\tilde{\omega}$ = nondimensional rotor speed, $=\omega/p_0$
ω_b = effective natural frequency of rotating blade, $\omega_b^2=p_{b_0}^2+\nu_0^2\omega^2$
ω_s = $\omega_s^2=p_{b_0}^2+\omega^2(\nu_0^2-1)$
$(\dot{})$ = differentiation with respect to time, t
$()'$ = differentiation with respect to nondimensionalized time, τ

Received Jan. 20, 1983; revision received Aug. 25, 1983.

*Assistant Professor, School of Mechanical Engineering.

Introduction

IT has been observed for approximately fifty years that vehicles having a rotor on a flexible support can experience a destructive instability known as ground resonance. The first vehicles to exhibit this phenomenon were the autogiros, followed in short order by the first helicopters.[1] The motion was initially thought to be a resonance between the ground and the rotorcraft, but in 1957 Coleman presented his now classic analysis of the process and showed it to be a self-excited instability.[2] Basically, some external disturbance will perturb the rotor blades. This moves their center of gravity off from the center of the rotor and so forms an inertial force which acts against the helicopter fuselage (Fig. 1). Since the fuselage is flexibly connected to the ground through the landing gear, the fuselage will start to rock. When the rotor speed is within a critical band of rotational speeds, this rocking will act to increase the amplitude of vibration that the blades are undergoing. This increased blade motion leads to a larger inertial force and one has an unstable situation between fuselage and blade motion. If left unchecked, the vibrations will increase until some nonlinear restoring force brings the system into a limit cycle or until some part of the rotorcraft fails.

Previous studies of ground resonance have concerned themselves with the purely linear problem,[2-7] i.e., their mathematical models employed linear springs and dampers. This paper will analyze a system in which *damping* nonlinearities are present and will examine the role of these nonlinearities in altering the system's response. Other possible nonlinearities are neglected in this basic study.

Figure 2 illustrates a simplified model of a helicopter. The fuselage, F, is constrained to translate along the x axis, giving it one degree of freedom. This motion represents the lateral motion of a helicopter on its landing gear.[3] The motion is constrained by a spring S and a damper D. The spring-damper combination represents the landing gear's resistance to lateral motions. A rigid, massless rotor R rotates at an angular speed

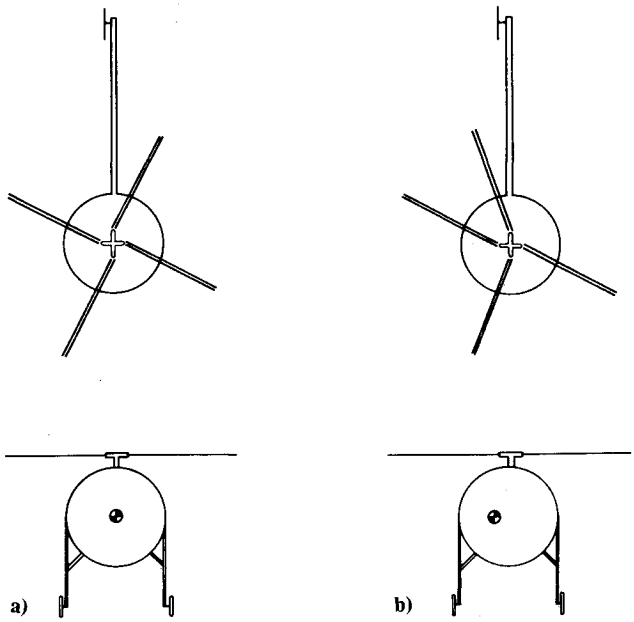

Fig. 1 a) Helicopter in a state of equilibrium; b) helicopter with one of its blades perturbed from equilibrium.

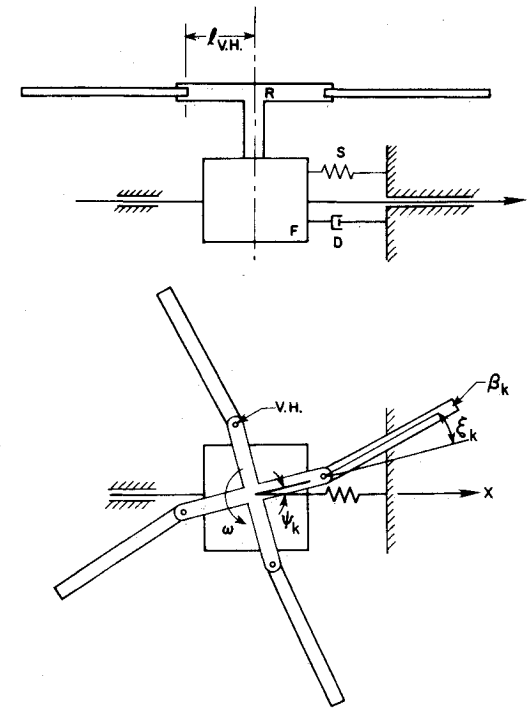

Fig. 2 Simplified model of a rotor on a movable fuselage.

ω and is supported by the fuselage. The blades (β_k) are attached to the rotor through vertical hinges, vh, and these hinges are offset from the central axis of the rotor by a distance ℓ_{vh}. The blades are rigid and they are constrained by the vertical hinge to move in a plane perpendicular to the angular velocity vector of the rotor. This type of blade motion is termed lag motion and the angular displacements of the blades are given by ξ_k. Only lag motions of the blades contribute substantially to the ground resonance phenomenon and so other degrees of freedom such as flap or twist are neglected.[2] ψ_k equals $\omega t+\alpha_k$ and gives the angular displacements of the different rotor arms. Aerodynamics are not important in ground resonance and are, therefore, neglected.[2]

The full equations of motion of the model are nonlinear. A linear analysis will neglect all but the first order terms. The *damping* nonlinearities considered in this paper are of the second order; it is, indeed, because of these that limit cycle behavior is observed. However, the second order *inertial* nonlinearities inherent in the original equations of blade motion are not retained in the following analysis. In the Appendix it is shown that retaining these terms will not affect the single frequency limit cycle behavior that is the object of study in this paper.

Analysis—Linear Theory

The following linear analysis follows that of Mil.[3] Applying D'Alembert's principle yields:

$$I\ddot{\xi}_k+2C_b\dot{\xi}_k+(K_b+\omega^2\ell_{vh}S)\xi_k=S\ddot{x}\sin\psi_k$$

$$M\ddot{x}+2C_0\dot{x}+K_0x=\frac{S}{M}\sum_{k=1}^{n}[(\ddot{\xi}_k-\omega^2\xi_k)\sin\psi_k+2\omega\dot{\xi}_k\cos\psi_k]$$

Dividing the first and second equation by I and M, respectively, and putting the equations in canonical form yields:

$$\ddot{\xi}_k+2n_b\dot{\xi}_k+\omega_b^2\xi_k=\frac{S}{I}\ddot{x}\sin\psi_k \tag{1}$$

$$\ddot{x}+2n_0\dot{x}+p_0^2x=\frac{S}{M}\sum_{k=1}^{n}[(\ddot{\xi}_k-\omega^2\xi_k)\sin\psi_k+2\omega\dot{\xi}_k(\cos\psi_k)] \tag{2}$$

The coupling between the fuselage and blades is now clear. Equation (2) is in the form of a normalized spring-mass-damper being driven by some force. n_0 is the damping coefficient and p_0 is the natural frequency of the fuselage-landing gear combination. Since $\psi_k=\omega t+\alpha_k$ the forcing function has an explicitly time-dependent part ($\sin\psi_k$ and $\cos\psi_k$) and also depends on the blade's displacement, velocity, and acceleration, as well as on the rotor speed ω. Similarly, the blade motion is described in Eq. (1) where n_b is the blade damping coefficient and ω_b^2 represents the blade's restoring spring. Note that $\omega_b^2=p_{b0}^2+\nu_0^2\omega^2$, where p_{b0}^2 represents an actual restoring spring, and $\nu_0^2\omega^2$ is the additional spring force due to centrifugal stiffening. The blades are driven by both the fuselage's acceleration and by the position of the blades ($\ddot{x}$, $\sin\psi_k$).

The problem with these equations is that they are variable-coefficient, linear-differential equations. It would be desirable to transform them into a constant coefficient form, since one could then use standard solution techniques such as the Laplace transform method. A possible transformation is to define two new variables such that:

$$\eta=\sum_{k=1}^{n}\xi_k\sin\psi_k \tag{3}$$

$$\phi=\sum_{k=1}^{n}\xi_k\cos\psi_k \tag{4}$$

η and ϕ represent motions of the center of mass of the blades. Since the center of mass is the driving force of the fuselage motion, it at least seems reasonable that such a transformation could be useful. Similar transformations exist that represent blade motions in which the center of mass remains fixed with respect to the fuselage.[8] To clarify the role of η and ϕ, one can examine the case of a four-blade rotor. For $\eta=4$, $\alpha_1=0$, $\alpha_2=\pi/2$, $\alpha_3=\pi$, $\alpha_4=3\pi/2$ and

$$\eta=\sin\omega t(\xi_1-\xi_3)+\cos\omega t(\xi_2-\xi_4) \tag{5}$$

$$\phi=\cos\omega t(\xi_1-\xi_3)-\sin\omega t(\xi_2-\xi_4) \tag{6}$$

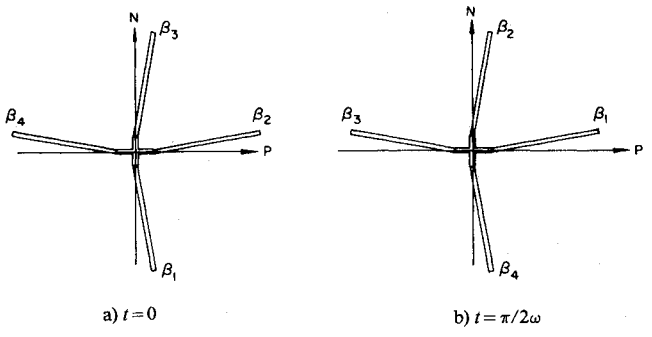

Fig. 3 Schematic showing how η and ϕ represent motions of the center of mass of opposed blades.

Let N and P represent a coordinate system originally aligned with the rotor and attached to the fuselage (Fig. 3). To begin, let $t=0$. One then has from Eqs. (5) and (6):

$$\eta=\xi_2-\xi_4, \quad \phi=\xi_1-\xi_3$$

From Fig. 3a it is clear that only blades 1 and 3 contribute to any movement of the center of mass along the P axis. Similarly, only movements of blades 2 and 4 will move the center of mass along the N axis. The position of the center of mass is (within a linear angular approximation) located at $\eta=(\xi_2-\xi_4)\ B$, $\phi=(\xi_1-\xi_3)\ B$, where B is the distance from an individual blade's center of mass to the blade's vertical hinge. Thus the above expressions for η and ϕ are seen to be proportional to the position of the center of mass of the blades. If $t=\pi/2\omega$ then:

$$\eta=\xi_1-\xi_3, \quad \phi=-(\xi_2-\xi_4)$$

and the rotor system rotates 90 deg to yield Fig. 3b. Note again that the expressions for η and ϕ are proportional to the position of the blades' center of mass.

Now that a physical feel for η and ϕ has been obtained, one can proceed to use them. If Eq. (1) is multiplied by $\cos\psi_k$ and summed from 1 to k, and similarly is multiplied by $\sin\psi_k$ and summed from 1 to k

$$\sum_{k=1}^{n}[\text{Eq. (1)}]\ \cos\psi_k=0, \qquad \sum_{k=1}^{n}[\text{Eq. (1)}]\ \sin\psi_k=0$$

the following equations result:

$$\ddot{x}+2n_0\dot{x}+p_0^2x-\frac{S}{M}\ddot{\eta}=0$$

$$\ddot{\eta}+2n_b\dot{\eta}+\omega_s^2\eta-2\omega(\dot{\phi}+n_b\phi)-\frac{n}{2}\frac{S}{I}\ddot{x}=0$$

$$\ddot{\phi}+2n_b\dot{\phi}+\omega_s^2\phi+2\omega(\dot{\eta}+n_b\eta)=0$$

where

$$\omega_s^2=p_{b0}^2+\omega^2(\nu_0^2-1)$$

Letting $\tau=p_0t$ and defining $\tilde{n}_0=n_0/p_0$, $\tilde{n}_b=n_b/p_0$, $\tilde{\omega}=\omega/p_0$ and $\tilde{\omega}_s=\omega_s/p_0$ yields

$$x''+2\tilde{n}_0x'+x-\frac{S}{M}\eta''=0 \tag{7}$$

$$\eta''+2\tilde{n}_b\eta'+\tilde{\omega}_s^2\eta-2\tilde{\omega}(\phi'+\tilde{n}_b\phi)-\frac{n}{2}\frac{S}{I}x''=0 \tag{8}$$

$$\phi''+2\tilde{n}_b\phi'+\tilde{\omega}_s^2\phi+2\omega(\eta'+\tilde{n}_b\eta)=0 \tag{9}$$

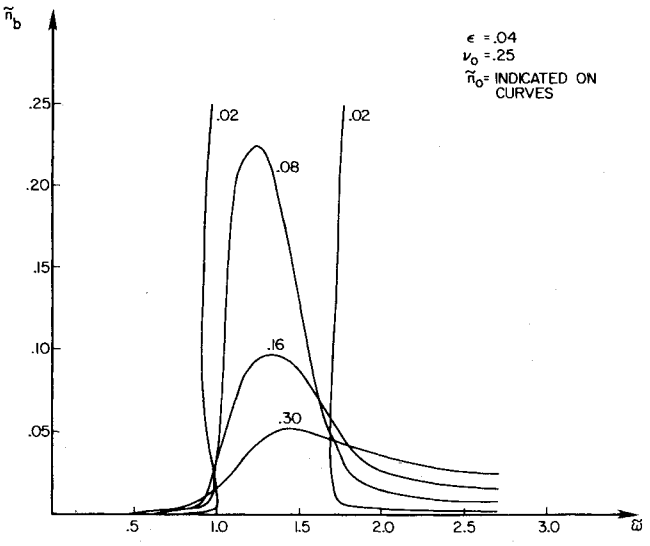

Fig. 4 Relation between $\tilde{n}_b$ (blade damping), $\tilde{n}_0$ (fuselage damping), and $\tilde{\omega}$ (rotor speed) for neutrally stable motion in a linear system.

One now has a set of linear, constant-coefficient, homogeneous equations which can easily be solved. To find the stability boundaries, let $x=X_0e^{i\tilde{a}\tau}$, $\eta=H_0e^{i\tilde{a}\tau}$ and $\phi=\Phi_0e^{i\tilde{a}\tau}$ where X_0, H_0, and Φ_0 are complex quantities and $\tilde{a}$ is real. Substituting these relations into Eqs. (7), (8), and (9) will yield a set of three linear algebraic equations

$$X_0(1-\tilde{a}^2+2i\tilde{a}\tilde{n}_0)+\frac{S}{M}\tilde{a}^2H_0=0 \tag{10}$$

$$H_0(\tilde{\omega}_s^2-\tilde{a}^2+2i\tilde{a}\tilde{n}_b)-2\tilde{\omega}\Phi_0(2\tilde{n}_b+i\tilde{a})+\frac{n}{2}\frac{S}{I}\tilde{a}^2X_0=0 \tag{11}$$

$$\Phi_0(\tilde{\omega}_s^2-\tilde{a}^2+2i\tilde{a}\tilde{n}_b)+2\tilde{\omega}H_0(2\tilde{n}_b+i\tilde{a})=0 \tag{12}$$

Setting the determinant of these equations to zero produces a sixth order, complex equation for the unknowns $\tilde{a}$ and $\tilde{\omega}$. The real and imaginary parts of this equation are individually equal to zero and so this complex equation can be written as two real equations

$$A_1\tilde{a}^6+A_2\tilde{a}^4+A_3\tilde{a}^2+A_4=0 \tag{13}$$

$$B_1\tilde{a}^4+B_2\tilde{a}^2+B_3=0 \tag{14}$$

where the A's and B's depend on the system parameters S, M, I, n, $\tilde{\omega}$, $\tilde{n}_b$, $\tilde{n}_0$, and $\tilde{\omega}_s$.

A quick way to analyze these equations is to note that Eq. (14) is second order in $\tilde{a}^2$. Therefore one can use Eq. (14) to solve for $\tilde{a}^2$. The resulting $\tilde{a}^2$ can then be inserted into Eq. (13) and the result examined. If it yields a result unequal to zero, $\tilde{\omega}$ is altered and the procedure is continued until both Eqs. (13) and (14) are satisfied. This allows one to obtain a plot similar to Fig. 4 in which the linear blade damping $\tilde{n}_b$ is plotted vs the rotor speed $\tilde{\omega}$ for all other parameters fixed. With this, one can predict the region of unstable $\tilde{\omega}$. For $\tilde{\omega}$ between $\tilde{\omega}_1$ and $\tilde{\omega}_2$, the motion variables have a form $x\sim e^{i\tilde{a}\tau}e^{b\tau}$. At $\tilde{\omega}_1$ and $\tilde{\omega}_2$ the response has the form $x\sim e^{i\tilde{a}\tau}$. Finally, for all other $\tilde{\omega}$ the form of the motion is $x\sim e^{i\tilde{a}\tau}\ e^{-b\tau}$, where a and b are real and greater than zero.

Analysis—Nonlinear Theory

The first extension to this linear theory is to model the landing gear damping as being composed of linear and nonlinear elements in parallel. In this analysis, the nonlinear

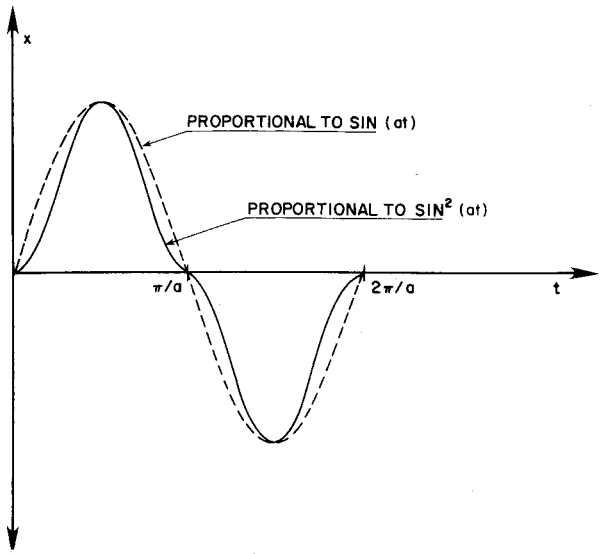

Fig. 5 Difference between a hydraulic damper ($\sin^2 at$) and a linear one ($\sin at$).

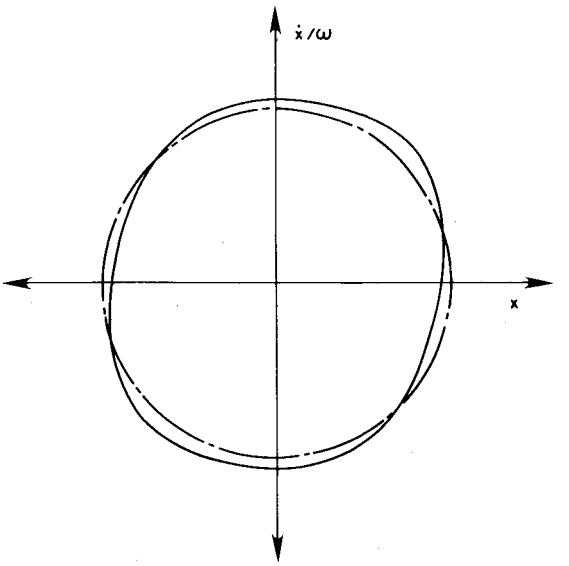

Fig. 6 Comparison between motion of nonlinear system (———) vs the quasilinearized system (– – –) with high level of nonlinearity present.

element is represented by $F_d=\gamma\dot{x}\,|\dot{x}|$, where γ controls the degree of nonlinearity in the system. Thus one now has:

$$\ddot{x}+2n_0\dot{x}+\gamma\dot{x}\,|\dot{x}|+p_0^2x=(S/M)\,\ddot{\eta} \tag{15}$$

$$\ddot{\phi}+2n_b\dot{\phi}+\omega_s^2\phi+2\omega(\dot{\eta}+n_b\eta)=0 \tag{16}$$

$$\ddot{\eta}+2n_b\dot{\eta}+\omega_s^2\eta-2\omega(\dot{\phi}+n_b\phi)=(nS/2I)\,\ddot{x} \tag{17}$$

These equations can now be rewritten by letting $\tau=p_0t$

$$x''+2\tilde{n}_0x'+\tilde{\gamma}x'\,|x'|+x=(S/M)\,\eta'' \tag{18}$$

$$\phi''+2\tilde{n}_b\phi'+\tilde{\omega}_s^2\phi+2\tilde{\omega}(\eta'+\tilde{n}_b\eta)=0 \tag{19}$$

$$\eta''+2\tilde{n}_b\eta'+\tilde{\omega}_s^2\eta-2\tilde{\omega}(\phi'+\tilde{n}_b\phi)=(nS/2I)x'' \tag{20}$$

Multiplying all three equations by γ and Eqs. (19) and (20) by S/M and defining $\tilde{x}=\gamma x$, $\tilde{\eta}=\eta\gamma(S/M)$ and $\tilde{\phi}=\phi\gamma(S/M)$ yields

$$\tilde{x}''+2\tilde{n}_0\tilde{x}'+|\tilde{x}'|\tilde{x}'+\tilde{x}=\tilde{\eta}'' \tag{21}$$

$$\tilde{\phi}''+2\tilde{n}_b\tilde{\phi}'+\tilde{\omega}_s^2\tilde{\phi}+2\tilde{\omega}(\tilde{\eta}'+\tilde{n}_b\tilde{\eta})=0 \tag{22}$$

$$\tilde{\eta}''+2\tilde{n}_b\tilde{\eta}'+\tilde{\omega}_s^2\tilde{\eta}-2\tilde{\omega}(\tilde{\phi}'+\tilde{n}_b\tilde{\phi})=\epsilon\tilde{x}'' \tag{23}$$

where

$$\epsilon=nS^2/2IM$$

The parameter γ has been eliminated and thus the solution of the equations will be valid for all values of γ. ϵ is an inertial parameter of the rotorcraft that depends on the number of blades, mass of the fuselage and blades, and mass distribution of the blades.

The equations of motion are now in their final form. Recall that $\tilde{n}_0$ and $\tilde{n}_b$ are nondimensional landing gear and blade damping coefficients, respectively. $\tilde{\omega}$ is the nondimensional rotor speed. $\tilde{\omega}_s^2$ appears as a nondimensional natural frequency. Note however, that from the previous definitions, $\tilde{\omega}_s^2=\tilde{p}_{b0}^2+\tilde{\omega}^2(\nu_0^2-1)$. ν_0^2 is of order 0.1 for modern helicopters and the blade restoring springs are weak or, more commonly, absent. (In this analysis the spring is absent.) Therefore $\tilde{\omega}_s^2$ will have a negative value. Thus one might immediately suspect the existence of unstable behavior. ϵ is a fixed inertial property of the rotorcraft structure. Lastly, $\tilde{x}$ represents a nondimensional motion of the fuselage and $\tilde{\phi}$ and $\tilde{\eta}$ are nondimensional, transformed blade coordinates.

Consider now the term $\tilde{x}'\,|\tilde{x}'|$. The physical nature of $\tilde{x}'\,|\tilde{x}'|$ vs $\tilde{x}'$ for $\tilde{x}'\sim\sin(\tilde{a}\tau)$ is shown in Fig. 5. This nonlinearity will be approximated by constructing a describing function for it.[9] For $\tilde{x}'\,|\tilde{x}'|$, assuming an $\tilde{x}$ motion of $\tilde{x}=|\tilde{X}|\cos(\tilde{a}\tau)$, on has:

$$F_d=\tilde{a}^2\,|\tilde{X}|^2\sin^2(\tilde{a}\tau);\quad \tau\le\pi/\tilde{a}$$

$$=-\tilde{a}^2\,|\tilde{X}|^2\sin^2(\tilde{a}\tau);\quad \pi/\tilde{a}\le\tau\le2\pi/\tilde{a}$$

Express F_d as

$$F_d=\sum_{n=1}^{\infty}b_n\sin(\tilde{a}n\tau)$$

then

$$b_n=\frac{\tilde{a}}{\pi}\int_0^{2\pi/\tilde{a}}F_d\sin(\tilde{a}n\tau)\,d\tau$$

Retaining the first harmonic produces

$$F_d=\frac{8}{3\pi}\tilde{a}^2\,|\tilde{X}|^2\sin(\tilde{a}\tau) \tag{24}$$

Note that the amplitude is nonlinearly related to the input (proportional to $\tilde{X}$ and $\tilde{a}$) but the output frequency is the same as the input frequency. It is for this reason that the method is often called quasilinearization; the approximation is not fully nonlinear, but is more than just linear.

The most important question at this point is whether this is a good approximation. A straightforward test is to run numerical simulations of the following two equations and compare the results.

$$\ddot{x}+b\dot{x}\,|\dot{x}|+\omega_n^2x=F\sin(\omega t) \tag{25}$$

$$\ddot{x}+\frac{8\omega Ab}{3\pi}\dot{x}+\omega_n^2x=F\sin\omega t \text{ where } x=A\sin(at+\beta) \tag{26}$$

By varying b, F, ω_n, and ω one can find how closely the response for Eq. (25) matches that of Eq. (26) over a range of input parameters.

An example of such a comparison in which the deviations are of a worst case type is shown in Fig. 6. The quasilinear response is in the form of a circle, so any noncircularity of the

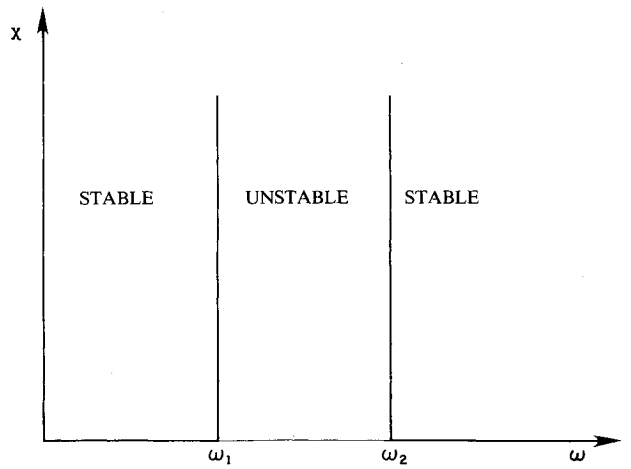

Fig. 7 Regions of instability and stability for linear case.

nonlinear response is due to the higher order terms generated by the nonlinear element. The main point is that even in this case, which is among the most nonlinear of the responses, the quasilinear approximation is still quite good. Noting this, one can proceed with the helicopter analysis.

Equation (21) is now modified by replacing $\tilde{x}'|\tilde{x}'|$ with $(8/3\pi)\tilde{a}|\tilde{X}|\tilde{x}'$:

$$\tilde{x}'' + \left[2\tilde{n}_0 + \frac{8\tilde{a}|\tilde{X}|}{3\pi}\right]\tilde{x}' + \tilde{x} = \tilde{\eta}'' \tag{27}$$

Once again assume motion of the form $\tilde{x}=\tilde{X}\,e^{i\tilde{a}\tau}$, etc., substitute these expressions into Eqs. (22), (23), and (27) and solve the resulting set of algebraic equations. The final characteristic equation is

$$\begin{aligned}
&\tilde{a}^6(1-\epsilon) - \tilde{a}^5(32\tilde{n}_b\tilde{X}/3\pi) - \tilde{a}^4[4\tilde{\omega}^2 + 4\tilde{n}_b(2\tilde{n}_0+\tilde{n}_b) \\
&\quad + 1 + \tilde{\omega}_s^2(2-\epsilon)] + \tilde{a}^3(\tilde{\omega}_s^2+2\tilde{\omega}^2)(32\tilde{X}\tilde{n}_b/3\pi) \\
&\quad + \tilde{a}^2[\tilde{\omega}_s^2(2+\tilde{\omega}_s^2+8\tilde{n}_0\tilde{n}_b) + 4\tilde{n}_b^2 + 4\tilde{\omega}^2(1+\tilde{n}_b^2+4\tilde{n}_b\tilde{n}_0)] \\
&\quad - \tilde{\omega}_s^4 - 4\tilde{\omega}^2\tilde{n}_b^2 - i[\tilde{a}^5(4\tilde{X}/3\pi) + \tilde{a}^4[\tilde{n}_b(2-\epsilon)+\tilde{n}_0] \\
&\quad - \tilde{a}^3(2\tilde{n}_b^2+\tilde{\omega}_s^2+2\tilde{\omega}^2)(8\tilde{X}/3\pi) - 2\tilde{a}^2[\tilde{\omega}_s^2(\tilde{n}_0+\tilde{n}_b) \\
&\quad + \tilde{n}_b(1+2\tilde{n}_0\tilde{n}_b) + 2\tilde{\omega}^2(\tilde{n}_b+\tilde{n}_0)] + \tilde{a}(\tilde{\omega}_s^4 + 4\tilde{n}_b^2\tilde{\omega}^2) \\
&\quad \times (4\tilde{X}/3\pi) + \tilde{\omega}_s^2(\tilde{\omega}_s^2\tilde{n}_0 + 2\tilde{n}_b) + 4\tilde{n}_b\tilde{\omega}^2(1+\tilde{n}_b\tilde{n}_0)] = 0
\end{aligned}$$

Note that this is sixth order in $\tilde{a}$, not third order in $\tilde{a}^2$ as before. Also, the $\tilde{X}$ amplitude now appears explicitly. This means that the limit cycle amplitude of the nonlinear system is directly related to $\tilde{a}$, the frequency of oscillation, and both must be solved for simultaneously.

In this study the Newton-Raphson method was used to solve the above equation. The real and imaginary parts of the characteristic equation define two new equations, f_1 and f_2, which are both set to zero. The Newton-Raphson procedure requires one to form $J(f_1,f_2)$ where J is defined as

$$J = \begin{bmatrix} \dfrac{\partial f_1}{\partial \tilde{X}} & \dfrac{\partial f_1}{\partial \tilde{a}} \\ \dfrac{\partial f_2}{\partial \tilde{X}} & \dfrac{\partial f_2}{\partial \tilde{a}} \end{bmatrix}$$

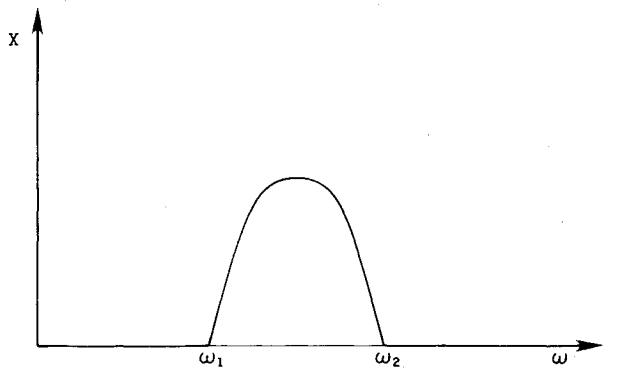

Fig. 8 Intuitively expected motion for limit cycle behavior when restoring nonlinearity is present in linear unstable regime.

The equations

$$[J]\begin{Bmatrix}\Delta\tilde{X}\\ \Delta\tilde{a}\end{Bmatrix} = -\begin{Bmatrix}f_1\\ f_2\end{Bmatrix},\quad \tilde{X}_{\text{new}} = \tilde{X} + \Delta\tilde{X},\quad \tilde{a}_{\text{new}} = \tilde{a}_0 + \Delta\tilde{a}$$

are then used to iterate an initial guess of $\tilde{a}_0$ and $\tilde{X}_0$ to the correct values of $\tilde{a}$ and $\tilde{X}$.

Results

Figure 7 illustrates the expected behavior for the linear case. $\tilde{\omega}_1 < \tilde{\omega} < \tilde{\omega}_2$ implies motion of the form $x \sim e^{i\tilde{a}\tau}e^{b\tau}$ and $\tilde{\omega}=\tilde{\omega}_1$ or $\tilde{\omega}_2$ implies motion of the form $x \sim e^{i\tilde{a}\tau}$. When a nonlinear restoring element is added, one would expect to find finite limit cycle behavior between $\tilde{\omega}_1$ and $\tilde{\omega}_2$ ($x \sim e^{i\tilde{a}\tau}$). Between $\tilde{\omega}_1$ and $\tilde{\omega}_2$ as ω approaches $\tilde{\omega}_1$ and $\tilde{\omega}_2$ the amplitude should decrease to zero since the linear destabilizing term, b, is approaching zero and so the motion is only weakly unstable. This means that only a small amplitude of oscillation is needed for the nonlinear term to balance out the unstable linear behavior. Correspondingly, one expects the maximum limit cycle amplitude to occur in the middle of the region between $\tilde{\omega}_1$ and $\tilde{\omega}_2$ since this is where the linear model shows the strongest unstable behavior (Fig. 8). Thus one could start the nonlinear search near $\tilde{\omega}_1$ in Fig. 8, where one expects $\tilde{X} \approx 0.0$ and the oscillation frequency, $\tilde{a}$, has the value found from a linear analysis. Once the combined solution of $\tilde{a}$ and $\tilde{X}$ for a given $\tilde{\omega}$ is known, $\tilde{\omega}$ can be incremented and the corresponding $\tilde{a}$ and $\tilde{X}$ determined.

In actuality, the simple behavior described above is only found for large values of blade damping (Fig. 9, $\tilde{n}_b = 0.20$). As the blade damping decreases, the absolute magnitude of the response increases, as expected (Fig. 9, $\tilde{n}_b = 0.10$). However, a surprising result is that the response eventually becomes triple valued and the range of limit cycle oscillations increases beyond $\tilde{\omega}_2$, the limit predicted by linear theory ($\tilde{n}_b = 0.04$ in Fig. 9).

Physically this means that hysteresis now exists in the amplitude response. Figure 10 illustrates this motion. If $\tilde{\omega}$ increases from zero, the amplitude builds to point A. Any further increment in $\tilde{\omega}$ will cause the response to drop down to B, which in addition to being a different amplitude also entails a new (lower) frequency of oscillation. Correspondingly, if the lower branch is being traversed, then when $\tilde{\omega}$ decreases below the speed corresponding to point C, the amplitude will increase dramatically (to D) and the frequency of oscillation will increase as well. Thus, when increasing or decreasing $\tilde{\omega}$ through these critical points, the response will change abruptly. This behavior would be quite disturbing to an operator since the craft would suddenly experience greatly increased (or decreased) shaking for a very small change in $\tilde{\omega}$. Note that points on the middle curve (between A and C) are

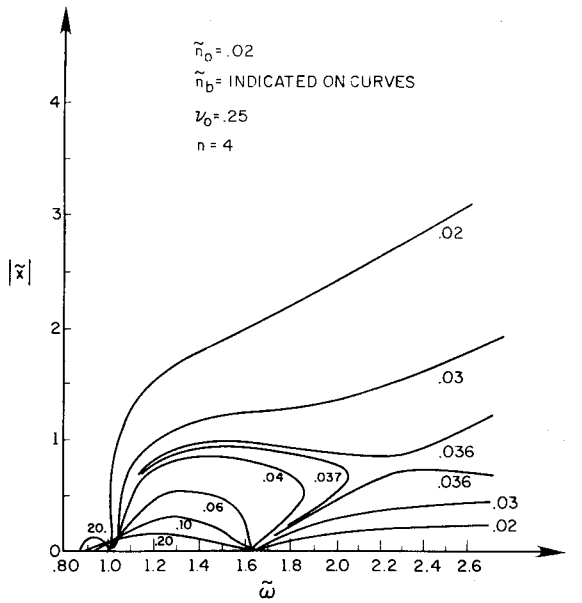

Fig. 9 Actual limit cycle behavior when hydraulic nonlinearity is present in the landing gear damper.

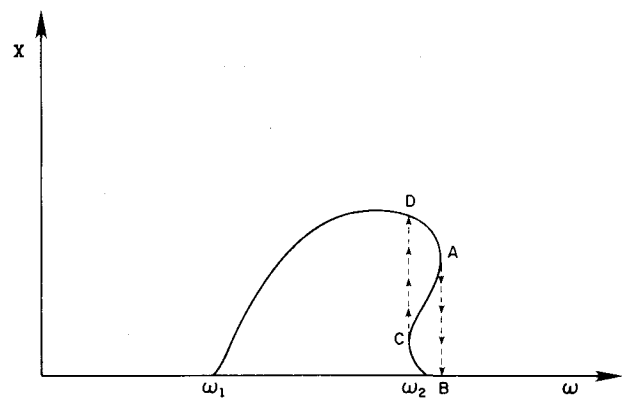

Fig. 10 Hysteretic response for triple-valued solution.

not physically realizable; they represent unstable limit cycles, and so motion that starts on this branch will jump to either the top or bottom branch. This alteration of stable and unstable limit cycles is quite common in nonlinear systems.[9] The lower branch of the triple valued curve is not visible in Fig. 9 due to its small magnitude relative to the other solutions.

An interesting numerical problem is how to solve for the unstable branch of the response. If $\tilde{\omega}$ is simply increased, the solution will drop to the lower branch upon moving beyond point A. One could attempt to jump directly onto the root by trial and error, but this is a very slow process. The method used to overcome this problem was to realize that plotting f_1 and f_2 as functions of $\tilde{a}$ and $\tilde{X}$ would yield a solution surface in the three-dimensional space defined by $f_1(\tilde{a},\tilde{X})$ and $f_2(\tilde{a},\tilde{X})$. By specifying $f_1 = f_2 = 0$, one cuts this surface and a curve similar to that illustrated in Fig. 11 is obtained. This curve shows the top and bottom branch solutions, as well as the middle one. These middle solution values can now be used as initial conditions for charting the unstable limit cycles. This method lends itself very well to a general search for solutions. If one has a solution for some value of $\tilde{a}$, then one can find all the other possible solutions by branching $f_1 = 0$ and $f_2 = 0$ from these initial values.

Returning to Fig. 9, if $\tilde{n}_b$ is further decreased, the response curves bifurcate ($\tilde{n}_b = 0.036$, Fig. 9). This is a fundamentally different behavior from that for larger $\tilde{n}_b$. For all larger values of $\tilde{n}_b$, the oscillations stop when one increases $\tilde{\omega}$ through the unstable regime. The transition to zero may be

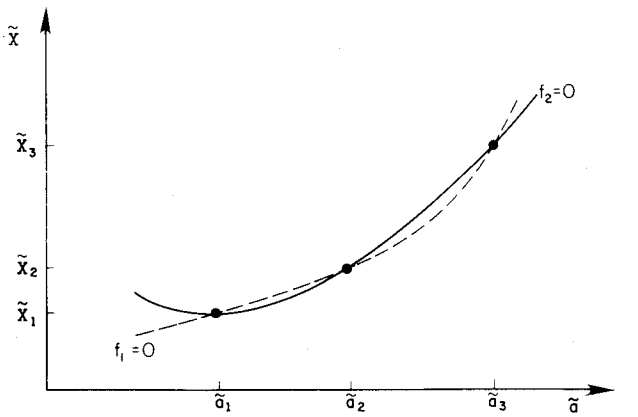

Fig. 11 Two solution functions f_1 and f_2 as functions of $\tilde{a}$ (frequency of oscillation) and $\tilde{X}$ (amplitude of fuselage motion).

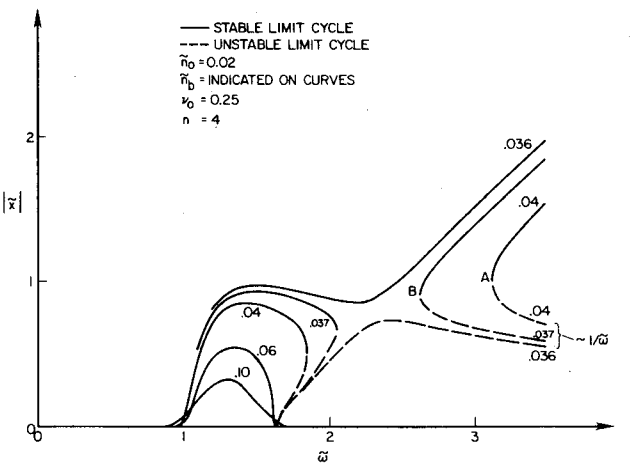

Fig. 12 Limit cycle behavior when hydraulic nonlinearity is present in the landing gear damper.

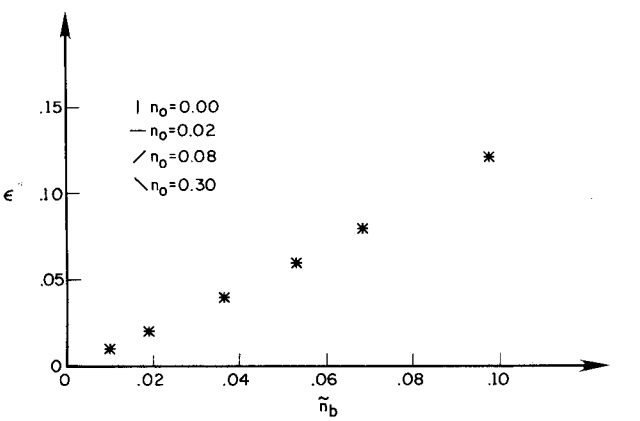

Fig. 13 Relation between ϵ (hinged mass ratio) vs $\tilde{n}_b$ (linear blade damping) required for bifurcation in solution curves.

gradual ($\tilde{n}_b = 0.10$) or abrupt ($\tilde{n}_b = 0.037$), but it always occurs. Now one has the situation in which the stable limit cycle will persist for all $\tilde{\omega} > \tilde{\omega}_1$. The bottom branch represents unstable limit cycle behavior which continues as $\tilde{\omega}$ approaches infinity. In this situation there exits no way to leave the top branch once it has been entered, except by reducing $\tilde{\omega}$ or by disturbing the system sufficiently strongly that the response moves through the middle branch to the underlying stable region.

The bifurcation phenomenon can be understood by extending the domain of input rotor speeds. Figure 12 illustrates

the response in this expanded range. Several points can now be made.

First, one notes that multiple limit cycle solutions exist over a greater range than previously indicated. Examine the case of $\tilde{n}_b = 0.04$, for example. It had appeared that for all rotor speeds above approximately 1.8, only a zero amplitude solution existed. Now it is seen that this is only true up to $\tilde{\omega} = 3.1$. Above this speed, multiple solutions exist, both stable and unstable. Figure 12, therefore, shows that the existence of a finite limit cycle solution is the rule rather than the exception, since only for two finite frequency intervals ($0 <$ lower limit of left solution branch and upper limit of left solution branch $<$ lower limit of right solution branch) can a zero amplitude solution exist with no associated finite limit cycle solutions.

Second, although the zero amplitude solution is stable for all rotor speeds above approximately 1.6, the stability becomes relatively weaker since the unstable locus (indicated by the dashed line) has an asymptotic behavior of the form, $\tilde{X} \sim 1/\tilde{\omega}$ as $\tilde{\omega} \to \infty$. Therefore, a progressively smaller perturbation to the system is required to drive the oscillation amplitude from zero, through the unstable locus and to the stable, high amplitude solution locus.

Third, as the damping decreases, the rotor speed at which the second solution branch occurs will decrease. For $\tilde{n}_b = 0.04$, point A indicates the lower rotor speed limit of the right branch. As $\tilde{n}_b$ is decreased to 0.037 the minimum speed of the right branch decreases, (shown in Fig. 12 by point B). Finally, for a level of damping between 0.036 and 0.037, the two branches touch. After this level of damping is passed, the loci join to form the previously noted bifurcation. Thus the locus at which the two branches join is analogous to the well-known separatrix, found in the phase plane representation of the solution of the equations of motion of a pendulum, in that it separates two distinct solution regions from each other.

A further interesting result is that the $\tilde{n}_b$ necessary for bifurcation is the same regardless of variations in $\tilde{n}_0$ (Fig. 13). If one wishes to eliminate the bifurcation phenomenon, one must increase $\tilde{n}_b$; altering $\tilde{n}_0$ will be ineffective. This is not at all intuitive. One would usually think that adding damping to either the blades or the landing gear would affect the response in some broadly similar way. However, analysis shows that even though the overall amplitude of the motion will change for varied $\tilde{n}_0$, the bifurcation itself will always occur for the same value of $\tilde{n}_b$. There is a final observation that is useful for determining the value of $\tilde{n}_b$ necessary for bifurcation. Figure 13 shows that the relation between ϵ and the value of $\tilde{n}_b$ necessary for bifurcation is quite linear. Therefore, one can predict the bifurcation $\tilde{n}_b$ from a knowledge of ϵ. Numerical integrations of the equations of motion were performed to verify the above results. As expected from the analysis of Eqs. (25) and (26), the amplitudes and frequencies found from numerical integrations agreed with the results of the harmonic balance procedure.

For typical dimensional values, and $\tilde{n}_b = 0.02$, the x oscillations range from 0 to 0.3 m and the blade lag oscillations range from 0 to 360 deg. For $\tilde{n}_b = 0.20$, x and ξ range from 0 to 1.3 cm and 0 to 2 deg, respectively. The distance from the center of rotation of the actual helicopter to its rotor hub is approximately 1.5 m. Thus it is clear that for certain parameter ranges the results may not always be physically meaningful. The size of the actual oscillations is dependent on the nondimensional parameter, γ. For a given helicopter, if the degree of nonlinearity in the landing gear is increased, γ will increase and the actual x and ξ corresponding to $\tilde{x}$, $\tilde{\eta}$, and $\tilde{\phi}$ will decrease. Therefore, the question of whether the above phenomena, such as bifurcation, will occur depends on the specific helicopter being examined.

Conclusions

By including nonlinearities in the helicopter model, one can predict both the frequency and amplitude of the solution. Moreover, the addition of a nonlinear element to the landing gear of a simplified helicopter model will cause large qualitative changes in the response curves fom those predicted by linear theory. For large values of linear blade damping, the response follows one's intuitive notion of how the limit cycles should behave. That is, within a critical band of rotor speeds, a finite amplitude limit cycle will exist, the amplitude of which will decrease as the rotor speed approaches these boundaries from within. For rotor speeds outside the instability range predicted by linear theory, the system will not support a limit cycle and disturbances to the system will decay. As blade damping is decreased however, new phenomena occur. The solutions become triple-valued, and finally bifurcate. Thus, when increasing the nondimensional rotor speed $\tilde{\omega}$ from zero, the response can include limit cycles that increase to a maximum and then smoothly decay to zero, solutions that abruptly jump to zero, and solutions that keep limit cycling for all $\tilde{\omega}$ above some critical value. This behavior has important consequences with regard to piloting a rotorcraft.

The most dramatic nonlinear feature of the solutions, the bifurcation, depends only on the blade damping and is independent of variations in fuselage damping. This phenomenon (and the bowing out of the solutions in the triple-valued response region) implies that the range of unstable rotor speeds can actually be greater than that predicted by linear theory. Thus linear theory will sometimes give overly optimistic results with regard to stability boundaries. The various values of $\tilde{n}_b$ which produce bifurcation can be easily predicted if one knows the parameter ϵ, which involves the parameters S, I, M, and n. Finally, the results must be translated back into dimensional quantities in order to determine their physical significance.

Future work will involve introducing a nonlinear blade, as well as a nonlinear fuselage, damper.

Appendix

The full nonlinear equations of motion corresponding to the model of Fig. 2, including blade nonlinearities and nonlinear fuselage damping, are

$$\ddot{\xi}_k + 2n_b\dot{\xi}_k + p_{b_0}^2\xi_k + \omega^2 v_0^2 \sin\xi_k = (S/I)\ddot{x}\sin(\psi_k + \xi_k)$$

$$\ddot{x} + 2n_0\dot{x} + \gamma\dot{x}|\dot{x}| + p_0^2 x = \frac{S}{M}\sum_{k=1}^{n}\left[\ddot{\xi}_k\sin(\psi_k+\xi_k) + (\omega+\dot{\xi}_k)^2\cos(\psi_k+\xi_k)\right] \quad \text{(A1)}$$

If all terms greater than second order are neglected and the previously used nondimensionalizations are used, the resulting equations are

$$\tilde{\xi}_k'' + 2\tilde{n}_b\tilde{\xi}_k' + (\tilde{p}_{b_0}^2 + \tilde{\omega}\nu_0^2)\tilde{\xi}_k = (S^2/IM)\tilde{x}''[\sin\psi_k + \sigma\cos\psi_k\tilde{\xi}_k]$$

$$\tilde{x}'' + \tilde{x}'|\tilde{x}'| + 2\tilde{n}_0\tilde{x}' + \tilde{x} = \sum_{k=1}^{n}[\sin\psi_k(\tilde{\xi}_k'' - \tilde{\omega}^2\tilde{\xi}_k) + \cos\psi_k(2\tilde{\omega}\tilde{\xi}_k')] + \sigma\sum_{k=1}^{n}\left[\sin\psi_k(-2\tilde{\omega}\tilde{\xi}_k'\tilde{\xi}_k) + \cos\psi_k\left(\tilde{\xi}_k''\tilde{\xi}_k - \tilde{\omega}^2\frac{\tilde{\xi}_k^2}{2} + \tilde{\xi}_k'^2\right)\right] \quad \text{(A2)}$$

where $\sigma = 1/\gamma(S/M)$.

To determine the importance of the second order blade inertial nonlinearities that occur in Eq. (A2), numerical simulations were run for the same input parameters as those used in Fig. 9. The outputs of the numerical runs were recorded for several cycles and then the Fourier series

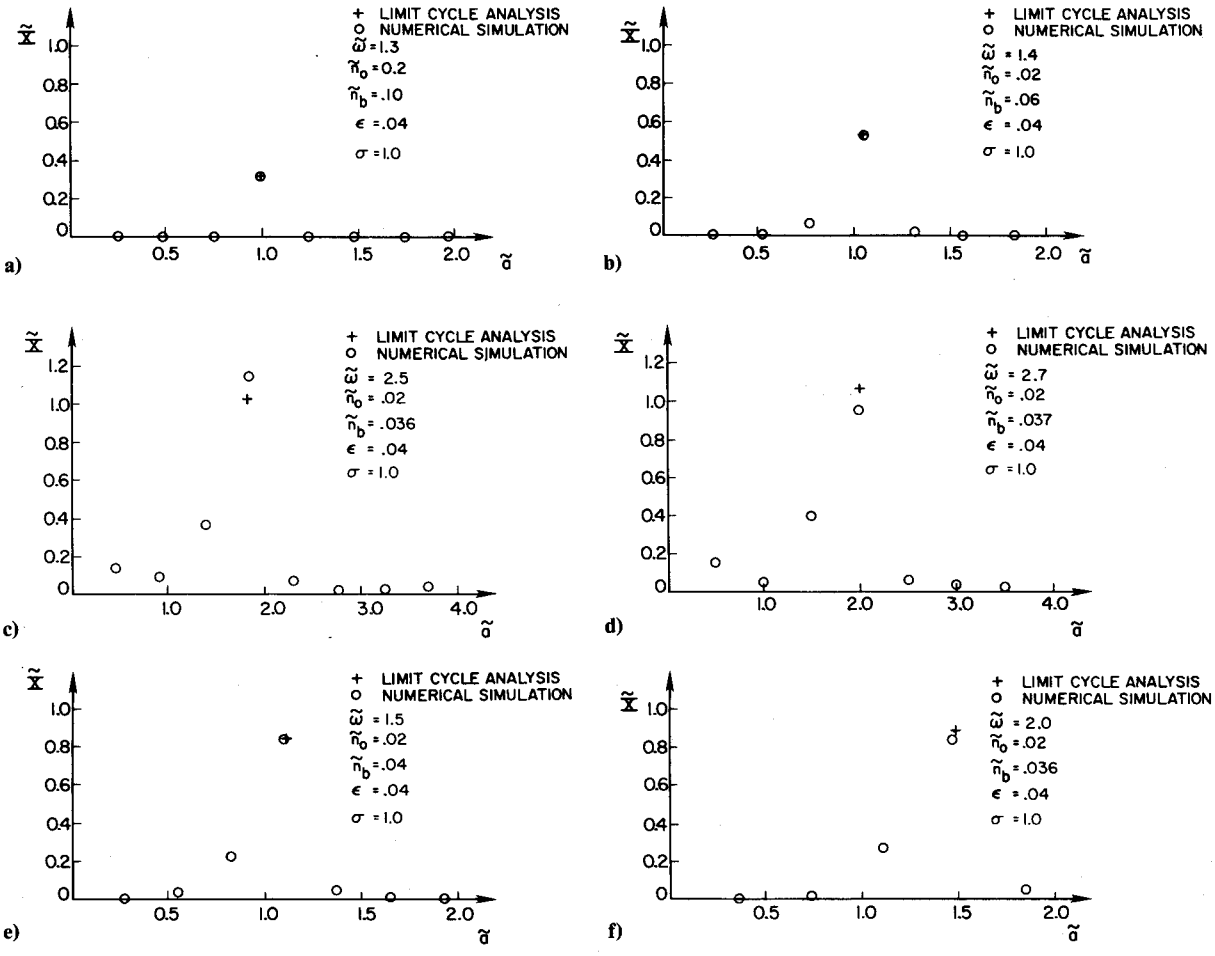

Fig. A1 Harmonic content of steady-state motion for limit cycle analysis and numerical simulation, amplitude vs frequency.

coefficients of the resulting data were calculated. The resulting amplitudes and frequencies present in the outputs are compared with the previous limit cycle results which neglected blade inertial nonlinearities in Fig. A1. As can be seen, the amplitude and frequency of the limit cycle motion found by the previous analysis remains relatively unchanged when blade inertial nonlinearities are included.

The major effect of the blade inertial nonlinearities is to increase the amplitude response of the offpeak frequencies which occur below the fundamental harmonic. Thus, the importance of these frequencies must be ascertained for the particular parameters being used.

Clearly, the results of the main paper are correct as far as the single frequency limit cycle response is concerned. In practice, one or two time simulations should be run to ensure that the limit cycle amplitude at the fundamental frequency is sufficiently large in comparison to the amplitude at other frequencies so that blade inertial nonlinearities may be neglected.

Acknowledgment

The author would like to thank Professors Earl H. Dowell and Howard C. Curtiss, Jr. for their invaluable advice during this investigation. Thanks must also go to Mr. Robert Blackwell of Sikorsky Aircraft Company for sharing some of his expertise. This work was supported by the National Science Foundation under Grant MEA-8119883 with the Division of Mechanical Engineering and Applied Mechanics.

References

[1]Gregory, H. F., *The Helicopter*, A. S. Barnes and Co. Inc., Cranburg, N.J., 1976, pp. 52,59.

[2]Coleman, R. P. and Feingold, A. M., "Theory of Self Excited Mechanical Oscillations of Helicopter Rotors with Hinged Blades," NACA Rept. 1351, Feb. 1957.

[3]Mil, M. L., Nekrasov, A. V., Grodko, L. N., Leykand, M. A., and Shurov, Z. Ye, "Helicopters—Calculation and Design," Vol. II, Vibrations and Dynamic Stability, NASA TT F-519, May 1968.

[4]Hammond, C. E., "An Application of Floquet Theory to Prediction of Mechanical Instability," *Journal of the American Helicopter Society*, Vol. 19, Oct. 1974, pp. 1-12.

[5]Peters, D. A. and Hohenemser, K. H., "Applications of the Floquet Transition Matrix to Problems of Lifting Rotor Stability," *Journal of the American Helicopter Society*, Vol. 16, April 1971.

[6]Gabel, R. and Capurso, V., "Exact Mechanical Instability Boundaries as Determined from the Coleman Equation," *Journal of the American Helicopter Society*, Vol. 7, Jan. 1962, pp. 17-21.

[7]Warming, T., "Some New Conclusions About Helicopter Mechanical Instability," *Journal of the American Helicopter Society*, Vol. 1, July 1956, pp. 1-9.

[8]Hohenemser, K. H. and Yin, S. K., "Some Applications of the Method of Multiblade Coordinates," *Journal of the American Helicopter Society*, Vol. 17, July 1972, pp. 3-12.

[9]Minorsky, N., *Theory of Nonlinear Control Systems*, McGraw-Hill Book Co., New York, 1969, pp. 64-66.